One-Dimensional Character of Combination Modes in the Resonance Raman Scattering of Carbon Nanotubes

C. Fantini,[1] A. Jorio,[1,4] M. Souza,[1] L. O. Ladeira,[1] A. G. Souza Filho,[2] R. Saito,[3] Ge. G. Samsonidze,[4] G. Dresselhaus,[4] M. S. Dresselhaus,[4] and M. A. Pimenta[1]

[1]*Departamento de Física, Universidade Federal de Minas Gerais, Caixa Postal 702, Belo Horizonte-MG 30123-970, Brazil*
[2]*Departamento de Física, Universidade Federal do Ceará, Fortaleza-CE, 60455-760, Brazil*
[3]*Department of Physics, Tohoku University and CREST JST, Aoba Sendai 980-8578, Japan*
[4]*Massachusetts Institute of Technology, Cambridge, Massachusetts, 02139-4307, USA*
(Received 24 September 2003; published 16 August 2004)

Resonance Raman spectroscopy with an energy tunable system is used to analyze the 600–1100 cm^{-1} spectral region in single-wall carbon nanotubes. Sharp peaks are associated with the combination of zone folded optic and acoustic branches from 2D graphite. These combination modes exhibit a peculiar dependence on the excitation laser energy that is explained on the basis of a highly selective resonance process that considers phonons and electrons in low dimensional materials.

Single-wall carbon nanotubes (SWNTs) are tiny tubules (~ 1 nm in diameter) formed by rolling up a graphene sheet [1]. Their physical properties depend on the rolling up geometry, described by the chiral vector $\mathbf{C_h} = n\mathbf{a}_1 + m\mathbf{a}_2 \equiv (n, m)$, where $\mathbf{a}_1$ and $\mathbf{a}_2$ are the unit cell basis vectors for the graphene sheet [2]. For example, SWNTs are metals if $\mathrm{mod}(2n + m, 3) = 0$ [3], and semiconducting otherwise. Therefore, it can be said that the Fermi level conductance of SWNTs can be turned on and off by changing the geometrical parameters, and this turn on/off property is a reflection of quantum confinement of the electronic structure in this one-dimensional (1D) system [2]. In this Letter we show that electronic scattering by phonons in SWNTs also exhibits a geometry based turn on/off effect.

The effect reported here is observed with a tunable Raman system used to characterize the phonon structure appearing at the intermediate frequency mode (IFM) region between 600 and 1100 cm^{-1} (see Fig. 1). This IFM spectral region is rich in Raman features but poorly studied. Previous work has highlighted that the IFM spectra are strongly dependent on the excitation laser line (E_{laser}) used to probe the SWNT sample, showing a frequency dispersive behavior with E_{laser} [4]. However, as shown here, a systematic study by using many laser lines very close in energy to each other reveals that the IFMs exhibit a new effect related to the 1D behavior of both electrons and phonons. The dispersive behavior is not monotonic, as observed for many features in graphitelike materials due to energy selective double-resonant Raman scattering processes [5,6], but it rather occurs in "steps," and we thus refer to this new effect here as a "steplike dispersive behavior."

The SWNT bundles were synthesized by an electric arc method in a He atmosphere using a Ni 2.1%/Co 2.1% catalyst. The diameter distribution of the sample is $d_t = 1.50 \pm 0.30$ nm, as obtained from the radial breathing

mode (RBM) frequency distribution [7]. Raman spectra were recorded in a backscattering configuration using a Dilor XY triple monochromator, equipped with a charge coupled device (CCD) and using 22 different laser line excitations from Ar, Kr, He-Ne and dye lasers focused on the sample with a $50\times$ objective, the power through the objective always being kept under 1 mW. Raman measurements were made at room temperature and ambient pressure.
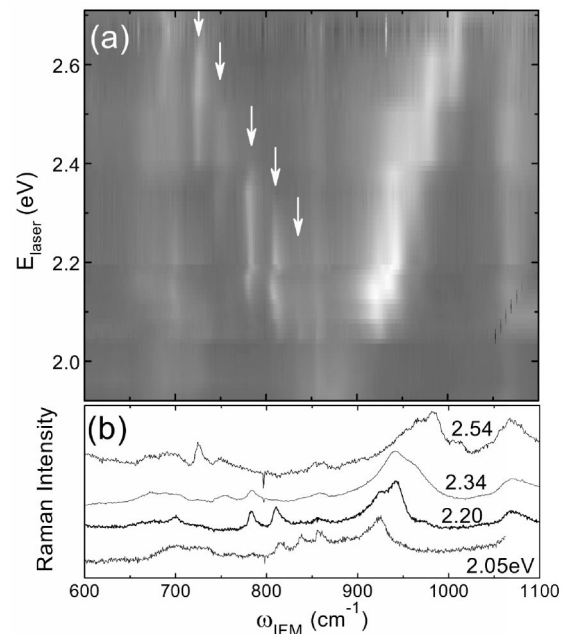

FIG. 1. (a) Two-dimensional plot for the E_{laser} dependence of the Raman spectra of SWNT bundles in the intermediate frequency mode (IFM) range. The light areas indicate high intensity. Arrows point to five well-defined ω_{IFM}^- features. (b) Raman spectra in the IFM range taken with $E_{\mathrm{laser}} = 2.05$, 2.20, 2.34, and 2.54 eV.

Figure 1(a) plots the E_{laser} dependence of the IFM features. This figure was constructed by taking IFM spectra obtained with 22 different E_{laser} values between 1.92 and 2.71 eV, and represents results that would be seen by a continuously tunable laser. The light areas in Fig. 1(a) indicate strong Raman intensities. The IFM Raman spectra obtained with $E_{laser} = 2.05$, 2.20, 2.34, and 2.54 are shown in Fig. 1(b) as examples. The spectra taken at various E_{laser}, as shown in Fig. 1, exhibit broad features at about 700, 860, and 1070 cm^{-1}, which are observed for every E_{laser} and are basically not dispersive, as well as features with a dispersive behavior, i.e., the frequencies change with changing E_{laser}. This Letter focuses on the IFMs with dispersive behavior.

Interestingly, the use of a tunable system and many (22) different laser lines, with a small energy spacing between them, brings into focus a new and very unusual effect for Raman spectroscopy, that is the discrete (steplike) dispersion of the IFM features. When E_{laser} is varied, individual Raman peaks first increase and then decrease in intensity, while remaining approximately constant in frequency. This behavior can be seen clearly by observing some of the well-resolved sharp peaks [see arrows in Fig. 1(a)]. For example, the peaks at 780 and 810 cm^{-1} can be observed, respectively, in the ranges $2.10 \leq E_{laser} \leq 2.40$ eV and $2.05 \leq E_{laser} \leq 2.35$ eV.

It is important to note that the appearance and disappearance of peaks in the IFM region cannot be explained by the usual resonance Raman effect, as is observed for first-order single-resonance modes in SWNTs, such as the RBMs [7]. A resonance Raman signal from SWNTs is observed when E_{laser} is very close to the energy E_{ii} between electronic van Hove singularities (vHSs) in the valence and conduction bands (the subscript index $i = 1, 2, 3, \ldots$ labels the electronic vHSs as their energy magnitude increases) [2]. Considering the sample d_t distribution and the E_{laser} values that were used, resonance with mostly the E_{33}^S and E_{44}^S electronic vHSs for semiconducting SWNTs can be achieved, as shown in Fig. 2(a). More than 50 different semiconducting SWNTs have their E_{33}^S and E_{44}^S energies within the experimental E_{laser} range, which means that the first-order single-resonance RBM spectra should be composed of about 50 different RBM peaks [7]. When looking at Fig. 1(a), it is clear that a very small number of IFM modes are observed [e.g., only five peaks, jumping to lower frequencies, as E_{laser} is increased; see arrows in Fig. 1(a)] and, therefore, the IFM features cannot be explained on the basis of a first-order single-resonance process.

Before discussing the specific selective process that leads to the steplike dispersive behavior observed in Fig. 1(a), it is necessary to identify the origin of the IFM features. In the 2D graphite parent material, the IFM spectral region is composed of an optical branch (here labeled $\mathcal{O}$) and by the acoustic branches (here labeled $\mathcal{A}$) [2]. In a second-order scattering process,

these modes can become Raman active, and the sum and difference of phonon frequencies can be observed. Such an effect is common in molecular spectroscopy but very unusual in solid state spectroscopy, where too many combinations are possible, and the averaging over many wave-vector-allowed processes gives rise to just a broad background rather than observable peaks with well-defined frequencies.

The IFMs can be related to the combination of two phonons that originate from a zone-folding procedure of two 2D phonon branches, one optical ($\mathcal{O}$) and one acoustic ($\mathcal{A}$). The $\mathcal{O}$ frequency $\omega_{\mathcal{O}}$ phonon exhibits a weak dispersion, whereas the $\mathcal{A}$ frequency $\omega_{\mathcal{A}}$ mode exhibits a stronger positive dispersion related to the speed of sound in 2D graphite [2] [see schema in Fig. 3(a)]. The sum $\omega_{IFM}^+ = \omega_{\mathcal{O}}^+ + \omega_{\mathcal{A}}^+$ (creation of two phonons) and the difference $\omega_{IFM}^- = \omega_{\mathcal{O}}^- - \omega_{\mathcal{A}}^-$ (creation of an $\mathcal{O}$ phonon
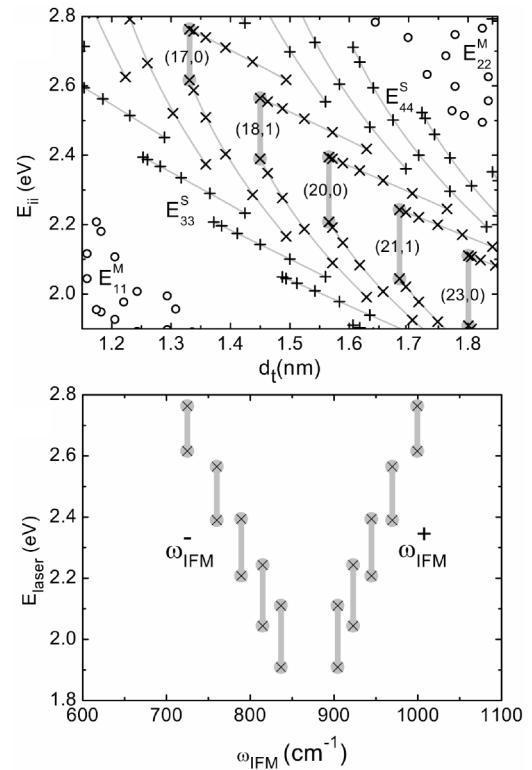

FIG. 2. (a) van Hove singularity (vHS) E_{ii} transition energies (from the tight binding model with $\gamma_0 = 2.9$ eV and $a_{C-C} = 0.142$ nm) as a function of d_t. The symbols "$\times$," "+," and "$\bigcirc$" stand for semiconducting $\text{mod}(2n + m, 3) = 1$, $\text{mod}(2n + m, 3) = 2$, and metallic SWNTs, respectively. Gray curves connect E_{ii}^S for SWNTs with $2n + m = $ const. The perpendicular broad gray lines are guides to the eye showing the connection between the E_{33}^S and E_{44}^S vHSs for selected (n, m) assigned SWNTs. (b) Theoretical prediction for the ω_{IFM}^+ and ω_{IFM}^- for special (n, m) SWNTs assigned in (a). Considering only the E_{33}^S and E_{44}^S vHSs for the SWNTs assigned in (a), the plot in (b) is constructed by considering $E_{laser} = E_{ii}$ and $\omega_{IFM}^\pm = \omega_0^\pm \pm v^\pm(6/d_t)$, $\omega_0^+ = 540$ cm^{-1}, and $\omega_0^- = 1195$ cm^{-1} (see text).

and annihilation of an $\mathcal{A}$ phonon) give rise to positively and negatively dispersive IFMs in Fig. 1(a), respectively.

Analysis of the average E_{laser} dependence for the IFMs (by "average" we mean that the steplike behavior is not taken into account) shows that their change in frequency ($\Delta\omega_{\text{IFM}}^{\pm}$) as the excitation laser energy is changed (ΔE_{laser}) is characterized by $\Delta\omega_{\text{IFM}}^{-}/\Delta E_{\text{laser}} \sim -220$ cm^{-1}/eV and $\Delta\omega_{\text{IFM}}^{+}/\Delta E_{\text{laser}} \sim +180$ cm^{-1}/eV, the different magnitudes being related to the small slope of the $\mathcal{O}$ phonon, and the average $\Delta\omega_{\mathcal{A}}/\Delta E_{\text{laser}} \sim 200$ cm^{-1}/eV gives the slope for the $\mathcal{A}$ phonon. In 2D graphite, the requirement for this second-order effect to become Raman active is just momentum conservation; i.e., the sum of the optical 2D wave vector ($\mathbf{q}_{2D}^{\mathcal{O}}$) and the acoustical 2D wave vector ($\mathbf{q}_{2D}^{\mathcal{A}}$) must be zero ($\mathbf{q}_{2D}^{\mathcal{O}} + \mathbf{q}_{2D}^{\mathcal{A}} = 0$).

When going from 2D graphite to 1D SWNT, the two-dimensional momentum conservation requirement in 2D graphite is translated into a 1D linear momentum conservation requirement along the tube axis plus angular momentum conservation around the nanotube axis. Furthermore, these selection rules become very selective in 1D systems because of the quantum confinement of the allowed wave vectors, forming the 1D van Hove singularities in the density of states. Normally, in the resonant Raman scattering process, either the incident or the scattered photon connects electronic states in E_{ii} vHSs in the valence and conduction bands. However, a very special case occurs when the electron excited at the E_{ii} vHS is scattered by a phonon to another electronic vHS state $E_{i'i'}$.

The phonon energies are small compared to electronic energies, and the closer in energy the E_{ii} and $E_{i'i'}$ electronic vHSs are, resonance can be achieved for the internal processes, and the higher the probability is for this scattering event to occur [5]. For the present experiment, resonance absorption and emission occurs in the E_{33}^{S} and E_{44}^{S} energy ranges [see Fig. 2(a)]. Because of the conservation of angular momentum requirement, these electronic states can only be connected by phonons with E_3 symmetry, where the phonon symmetry E_{μ} is determined by the number of complete wavelengths for atomic displacements around the nanotube circumference, where $\mu = 1, 2, 3$ for $1, 2, 3$ wavelengths [2]. For example, for a $(20, 0)$ SWNT, the E_{33}^{S} and E_{44}^{S} electronic states have $E_{\mu} = E_{12}$ and $E_{\mu'} = E_{15}$ symmetries, respectively, so that $E_{\mu''} = E_3$ is necessary for angular momentum conservation ($\mu - \mu' = \mu''$). However, due to Raman selection rules, E_3 symmetry modes cannot be observed in a first-order Raman scattering process [8,9], but can only be observed in a second-order scattering process involving two E_3 phonons, so that angular momentum is conserved.

The steplike dispersive IFM features are, therefore, related to the combination of two E_3 symmetry modes resonantly connecting two vHS electronic states. One of these phonons originates from the folding of the optical branch and one from the folding of one acoustic branch in 2D graphite. This process, however, can occur in many (n, m) SWNTs and several IFMs should be expected. The observation of a small number of IFMs indicates that another constraint must be introduced to explain the experimental observation.

The relation between the 2D phonon dispersion and the 1D SWNT structure comes from the zone-folding procedure [2]. If we consider an unrolled SWNT, it is possible to assign a wave vector $q_{\perp}$ perpendicular to the nanotube axis, i.e., along the nanotube circumference, given by $q_{\perp} = 2\pi/\lambda = 6/d_t$, since E_3 symmetry modes exhibit three complete wavelengths λ along the circumferential direction. The $\mathcal{A}$ dispersive behavior can be written as a function of $q_{\perp}$ instead of E_{laser} as $\omega_{\mathcal{A}} = v q_{\perp}$, by considering the resonance of the laser photon with the E_{33}^{S} vHSs. The average value $v \sim 2 \times 10^4$ m/s is obtained from the experimental dispersion, in accordance with the in-plane velocity of sound in graphite [2].

Figure 2(a) can be directly related to experimental results shown in Fig. 1. The y axes energy ranges in Fig. 2 can be related by $E_{\text{laser}} = E_{ii}$ for resonance conditions. The x axis d_t can be transformed into ω_{IFM} considering $\omega_{\text{IFM}}^{\pm} = \omega_0^{\pm} \pm v^{\pm} q_{\perp}$, while $q_{\perp} = 6/d_t$ for the special phonons, as discussed above. This transformation applies only to the E_{33}^{S} and E_{44}^{S} vHSs for the specific SWNTs assigned in Fig. 2(a), and the result for those special SWNTs is shown in Fig. 2(b). The similarity between Fig. 2(b) and the "V" picture observed in Fig. 1(a) indicates that the steplike dispersive IFMs come from these specific (n, m) SWNTs with mod($2n + m, 3$) = 1 having chiral angle θ very close to zero.

To understand this selective observation of IFM features related to $\theta \to 0$ SWNTs, the *phonons* vHSs are considered. As shown in Fig. 3(a), the 1D phonon struc-
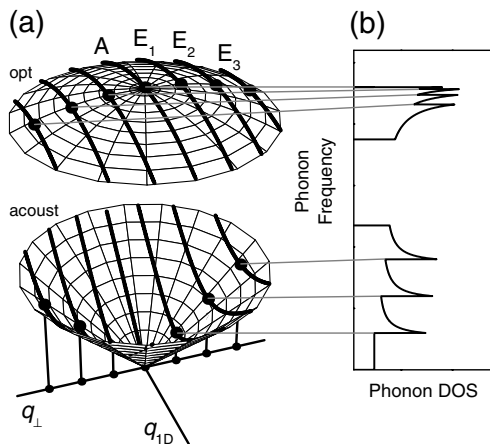

FIG. 3. (a) Schema for the 2D phonon dispersion of one acoustic and one optical phonon branch close to the Γ point. The cutting lines represent the allowed 1D wave vectors for a given (n, m) SWNT. The symmetry for each cutting line is indicated close to the optical modes. (b) Phonon density of states showing the confinement of phonon states at the 1D vHSs, that occurs at $q_{1D} = 0$.

ture gives rise to cutting lines of allowed 1D wave vectors (q_{1D}) parallel to the nanotube axis, while the wave vector perpendicular to the nanotube axis ($q_\perp$) is quantized and described by the different phonon symmetries (A, E_1, E_2, E_3, etc.) related to their angular momentum. The cutting lines give rise to 1D vHSs in the phonon density of states when $q_{1D} \to 0$.

When the electron is scattered by the phonon, the linear momentum conservation requirement can be written as $|q_{1D}| = |k_f - k_i|$, where q_{1D}, k_i, and k_f represent the 1D wave vectors (along the nanotube axis) for the phonon, and for the initial and final electronic states, respectively. By considering the Raman signal to be related to the scattering of electronic states at the *electronic* vHSs, E_3 symmetry phonons with wave vector $|q_{1D}| = |k_4 - k_3|$ should be considered, where k_3 and k_4 describe wave vectors for electronic states at the E_{33}^S and E_{44}^S vHSs, respectively. Why only k_3 and k_4 need to be considered is related to the quantum confinement of a large density of electronic states at the vHSs.

When considering 1D phonon structure, i.e., the high density of phonons states have $q_{1D} \to 0$ (see Fig. 3), the IFM Raman signal must be related to specific SWNTs for which E_{33}^S and E_{44}^S exhibit similar electronic wave vectors (i.e., $k_3 \approx k_4$), so that for momentum conservation, the special phonons that scatter electrons between these electronic states exhibit phonon wave vectors $|q_{1D}| = |k_4 - k_3| \to 0$, i.e., they are at the vHSs ($q_{1D} = q_{vHS}$). Because of the geometric structure of carbon nanotubes [2], $k_4 \approx k_3$ occurs for $\theta \to 0$ SWNTs, and $k_4 \equiv k_3$ only occurs for $\theta = 0$, i.e., for $(n, 0)$ zigzag SWNTs.

Five ω_{IFM}^- and five ω_{IFM}^+ peaks are observed in Fig. 1(a), and they are related to the five $\theta \to 0$ SWNTs assigned in Fig. 2(a). Only $\text{mod}(2n + m, 3) = 1$ SWNTs ["$\times$" in Fig. 2(a)] contribute to the Raman spectra because the probability for the scattering event to occur is much higher for the $\text{mod}(2n + m, 3) = 1$ SWNTs than for the $\text{mod}(2n + m, 3) = 2$ SWNTs ["+" in Fig. 2(a)], since $\text{mod}(2n + m, 3) = 1$ SWNTs exhibit a much smaller energy difference between E_{33}^S and E_{44}^S vHSs. The ω_{IFM}^+ are not as clearly separated in frequency as the ω_{IFM}^- peaks [see Figs. 1(a) and 2(b)], because of the small negative dispersion of the $\mathcal{O}$ modes. The ω_{IFM}^+ features exhibit larger intensity because they are related to the $\mathcal{A}$-mode *Stokes* process (creation of an $\mathcal{A}$ phonon), while the ω_{IFM}^- features are related to the less probable $\mathcal{A}$-mode *anti-Stokes* process (annihilation of an $\mathcal{A}$ phonon).

In summary, in the 1D carbon nanotubes, the electrons and phonons are confined in 1D channels (the van Hove singularities) that can only be efficiently connected under very specific geometrical arrangements. In the present study, specific electron-phonon scattering is observed to be effective only for low chiral angle SWNTs because the

1D structure of SWNTs confines the phonon states at $q_{1D} = q_{vHS} \to 0$, and only low chiral angle SWNTs ($\theta \to 0$), for which the E_{33}^S and E_{44}^S electronic vHS states exhibit similar wave vectors ($k_3 \approx k_4$), can exhibit an efficient Raman scattering process with momentum conservation $|q_{1D}| = |k_4 - k_3| \to 0 = |q_{vHS}|$.

These new concepts from low dimensional systems can be used reciprocally to learn about phonon properties in its higher dimensional parent material graphite, properties that could not be learned by probing the high dimensional system due to the averaging on many wave-vector-allowed processes. In this case, resonance Raman spectroscopy turns out to be a powerful tool for enabling phonon studies, revealing new concepts related to the quantum confinement of phonons in low dimensional systems, so that the crystalline systems exhibit spectroscopic behavior similar to molecular systems. The present work shows the importance of phonon vHSs, which should also be considered for interpreting other resonance Raman scattering processes in carbon nanotubes, including the well studied D and G' bands [2], and for studying other related physical properties.

---

[1] S. Iijima, Nature (London) **354**, 56 (1991).
[2] R. Saito, G. Dresselhaus, and M. S. Dresselhaus, *Physical Properties of Carbon Nanotubes* (Imperial College, London, 1998); S. Reich, C. Thomsen, and J. Maultzsch, *Carbon Nanotubes* (Wiley-VCH, Weinheim, 2004).
[3] The $\text{mod}(2n + m, 3)$ is defined as the integer remaining from the division of $2n + m$ by 3. Other groups have used $\text{mod}(n - m, 3)$, that is equivalent, although $\text{mod} = 1$ and $\text{mod} = 2$ are interchanged. We use $2n + m$ since these families are related to other important physical properties.
[4] L. Alvarez *et al.*, Chem. Phys. Lett. **316**, 186 (2000).
[5] C. Thomsen and S. Reich, Phys. Rev. Lett. **85**, 5214 (2000).
[6] R. Saito *et al.*, Phys. Rev. Lett. **88**, 027401 (2002).
[7] M. Milnera *et al.*, Phys. Rev. Lett. **84**, 1324 (2000).
[8] T. Vuković *et al.*, Phys. Rev. B **65**, 045418 (2002).
[9] A. Jorio *et al.*, Phys. Rev. Lett. **90**, 107403 (2003).